Published in final edited form as:
*Langmuir*. 2013 January 15; 29(2): 710–716. doi:10.1021/la3037007.

# Superparamagnetic Iron Oxide Nanoparticles with Variable Size and an Iron Oxidation State as Prospective Imaging Agents

**Pavel Kucheryavy**[†], **Jibao He**[‡], **Vijay T. John**[‡], **Pawan Maharjan**[§], **Leonard Spinu**[‖], **Galina Z. Goloverda**[†], and **Vladimir L. Kolesnichenko**[*,†]

[†]Chemistry Department, Xavier University, New Orleans, Louisiana 70125, United States

[‡]Department of Chemical and Biomolecular Engineering, Tulane University, New Orleans, Louisiana 70118, United States

[§]Advanced Materials Research Institute University of New Orleans, New Orleans, Louisiana 70148, United States

[‖]Department of Physics, University of New Orleans, New Orleans, Louisiana 70148, United States

## Abstract

Magnetite nanoparticles in the size range of 3.2-7.5 nm were synthesized in high yields under variable reaction conditions using high-temperature hydrolysis of the precursor iron(II) and iron(III) alkoxides in diethylene glycol solution. The average sizes of the particles were adjusted by changing the reaction temperature and time and by using a sequential growth technique. To obtain $\gamma$-iron(III) oxide particles in the same range of sizes, magnetite particles were oxidized with dry oxygen in diethylene glycol at room temperature. The products were characterized by DLS, TEM, X-ray powder diffractometry, TGA, chemical analysis, and magnetic measurements. NMR $r_1$ and $r_2$ relaxivity measurements in water and diethylene glycol (for OH and $CH_2$ protons) have shown a decrease in the $r_2/r_1$ ratio with the particle size reduction, which correlates with the results of magnetic measurements on magnetite nanoparticles. Saturation magnetization of the oxidized particles was found to be 20% lower than that for $Fe_3O_4$ with the same particle size, but their $r_1$ relaxivities are similar. Because the oxidation of magnetite is spontaneous under ambient conditions, it was important to learn that the oxidation product has no disadvantages as compared to its precursor and therefore may be a better prospective imaging agent because of its chemical stability.



[*]Corresponding Author: vkolesni@xula.edu.

Supporting Information: TEM images of nanoparticles. Histograms of the number of particles versus particle size for different nanoparticles. Powder X-ray diffractograms, magnetization versus field curves, and magnetization versus temperature curves for nanoparticles. This material is available free of charge via the Internet at http://pubs.acs.org.

**Notes**: The authors declare no competing financial interest.

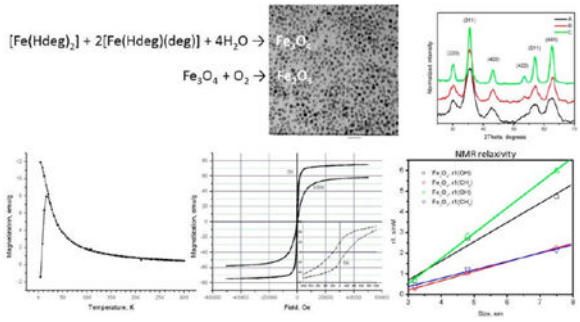


## 1. Introduction

Iron oxides and transition-metal ferrites with cubic structure are the focus of extensive basic and applied research because of their useful ferrimagnetic properties. These properties arise from a disproportion in the number of ferromagnetically coupled metal ions in two sublattices whose net moments are oriented oppositely. A sublattice formed by metal ions located in octahedral holes of the fcc oxygen framework counts twice as many metal ions as another sublattice, which is formed by ions located in tetrahedral holes of the same framework.[1] Changing the unpaired electron count in each sublattice is one of the ways to tune the magnetic properties of this and other spinel-structured materials.

The conversion from bulk to the reduced-dimension crystalline form (nanometer scale) causes the competition between the thermal energy and the magnetocrystalline anisotropy energy, which results in the transition from the ferromagnetic to superparamagnetic state when the vector of magnetization fluctuates in the absence of an external magnetic field. This transition takes place at the blocking temperature $T_b$, which is proportional to the particle volume and magnetic anisotropy. Another important difference between the macro-scale and nanoscale magnetic solids is that smaller particles may be less magnetic than the same material in bulk form because they contain a substantially greater fraction of metal ions located on the crystal surface, which may not contribute to the particle's net magnetization.[1,2]

The physics of nanoscale magnetic materials combined with their colloid and surface chemistry puts these materials on the front line of current research, in particular, that aimed at the development of ultracompact information storage and microelectronics on one side and labeling, imaging, delivery, and other therapeutic tools for biology and medicine on the other side.

The application of superparamagnetic iron oxide nano-particles in biology and medicine finds its rapidly developing emphasis on contrast agents for MRI.[3-8] Positive contrast imaging is frequently preferred in diagnostic practice; however, the existing gadolinium-containing $T_1$ contrast agents raise substantial toxicity issues[9] and their high mobility shortens their presence in the vascular system. These drawbacks of the gadolinium contrast agents motivate researchers' effort in the development of $T_1$ contrast agents based on ultrasmall superparamagnetic iron oxide particles.[10–14]

Because of their high magnetic moment, superparamagnetic nanoparticles enhance proton relaxation predominantly via an outer-sphere mechanism and therefore act as negative ($T_2$) contrast agents. In so-called positive ($T_1$) contrast agents, the inner-sphere relaxation mechanism is utilized because of the interaction of protons with high-spin $d^5$ transition-metal ions such as $Mn^{II}$ and $Fe^{III}$ or, more commonly, the $f^7$ $Gd^{III}$ ions.

The best currently known blood pool MRI agents are based on iron oxides and are considered to be nontoxic. Reducing the particle size to below 5 nm can lower their magnetic moment and therefore the outer-sphere relaxivity $r_2$.[11] At the same time, a larger surface-to-volume ratio of these small particles can cause a greater involvement of the iron atoms in the spin– lattice relaxation process, which relies on direct water coordination and exchange at the metal sites. Consequently, the particle size reduction can be the way to obtain a better $T_1$ contrast agent. One of the goals of this work was to study how the particle size and magnetization affect the relaxivity properties. We intentionally used no capping ligands or surfactants to make sure they would not interfere with water coordination and exchange at the particle's surface, which is important for accurate $T_1$ measurements.

It is known that magnetite spontaneously oxidizes in air, yielding $\gamma$-iron(III) oxide with a similar crystal structure. The similarity of their structures reflects on the magnetic properties: maghemite ($\gamma$-$Fe_2O_3$) has a saturation magnetization that is ~80% of the value for magnetite.[1] It could be expected that particles with the same size but various oxidation states of iron would show different $r_2$ relaxivities proportional to their magnetic moments. The $r_1$ relaxivities of magnetite and maghemite could be very diverse, however, because of their different surface chemistry and physics. Study on how the iron oxidation state affects the magnetic and relaxivity properties of the nanoparticles was another goal of this work.

## 2. Materials And Methods

### 2.1. Materials

Diethylene glycol 99%, anhydrous iron(III) chloride, and iron(II) chloride were purchased from Sigma-Aldrich and used with no additional purification. Diethylene glycol was degassed in a dynamic fore-vacuum with vigorous stirring for 1 h prior to use. Sodium metal and oleic acid were purchased from Fisher Scientific. Anhydrous ethyl acetate was purchased from Acros Organics and stored in a Schlenk bottle under nitrogen. Methanol was distilled in an inert atmosphere over sodium metal and stored in a Schlenk bottle under nitrogen. All reactions and operations with magnetite nanoparticles were performed with the rigorous exclusion of air and water using a Schlenk line and techniques involving an ultrapure-nitrogen-filled glovebox.

### 2.2. Methods

DLS measurements were carried out on a Zetasizer Nano ZS instrument (Malvern) in diethylene glycol, toluene, or water in 1 cm glass cuvettes at concentrations of ~0.7 mmol/kg. Powder X-ray diffractograms for isolated nanosolids were obtained using a Rigaku MiniFlex II X-ray diffractometer. The particle size and peak positions were obtained from X-ray diffraction patterns with Jade 8 software. TEM images were obtained for nanoparticles coated with oleic acid on a JEOL JEM 2010 transition electron microscope. The iron oxide content was determined by thermogravimetric analysis (TGA) with a Perkin-Elmer STA 6000 instrument.

$T_1$ and $T_2$ relaxation time measurements were performed at 297 °C using T1IR and CPMG pulse programs, respectively, on a Bruker Fourier 300 NMR spectrometer. Sample concentrations were in the range of $1 \times 10^{-4}$ to $3 \times 10^{-3}$ mmol/g in diethylene glycol and $1 \times 10^{-4}$ mmol/g to $3 \times 10^{-3}$ mmol/g in $D_2O$ in the presence of $H_2O$ (50 mg/2 g). $D_2O$ in a coaxial sealed tube was used to lock the NMR signal in diethylene glycol. All samples in diethylene glycol were prepared in a nitrogen-filled glovebox. The following equations were used for the calculations of $r_1$ and $r_2$ relaxivity:

$$\frac{1}{T_{1[\mathrm{Fe}]}}=\frac{1}{T_1}+r_1[\mathrm{Fe}] \text{ and } \frac{1}{T_{2[\mathrm{Fe}]}}=\frac{1}{T_2}+r_2[\mathrm{Fe}]$$

Magnetic studies were performed on a Princeton Measurements vector vibrating sample magnetometer (VSM) and on a Quantum Design MPMS-XL SQUID susceptometer. The samples were prepared as solid solutions of oleate-capped particles (5 wt %) in paraffin wax.

### 2.3. Synthesis

All reagents were used in the form of stock solutions in diethylene glycol: $FeCl_3$ and $FeCl_2$, 0.5 mol/kg each; $H_2O$, 1 mol/kg; and NaHdeg, 1.3 mol/kg (obtained by reacting Na metal with diethylene glycol). In a typical procedure, solutions of $FeCl_3$, $FeCl_2$, $H_2O$, and NaHdeg were mixed in the following proportion: 6 g (3 mmol) + 3 g (1.5 mmol) + 7 g (7 mmol) + 10 g (13 mmol).

The obtained green-brown solution was stirred overnight, transferred to a syringe, and then rapidly (2 s) injected into diethylene glycol (64 g) that had been preheated to a specified temperature. The overall iron concentration in the obtained colloids was 0.05 mol/kg.

For the synthesis of regularly sized nanoparticles (4.8 nm), the temperature of the preheated solvent was 245 °C. After the injection, it decreased to 190 °C and was maintained at this level for 1 h. Then the temperature was raised within 30 min to 210 °C and maintained at 210–220 °C for 1 h.

For the synthesis of smaller (3.2 nm) nanoparticles, the temperature of the preheated solvent was 220 °C. After the injection, it decreased to 180 °C, and the solution was held at this temperature for 1 h.

For the synthesis of larger (7.5 nm) nanoparticles, a new portion of the precursor solution (9 mmol of Fe) was added to the colloid of 4.8 nm particles at ~100 °C, followed by a slow temperature increase to 160 °C and then (in 30 min) to 210 °C, which was maintained at this level for another 30 min. Two other additions of the precursor solution and reheating resulted in the partial precipitation of the agglomerated magnetite. After its separation by using magnet, the clear colloid obtained was used for all studies.

Colloids of $\gamma$-iron(III) oxide were obtained by room temperature oxygenation of the magnetite colloids with dry $O_2$ for 1 week. Vigorous stirring helped to speed up the process. During oxygenation, the color of the solutions changed from brown-black to deep orange-brown.

A relatively small portion of each colloid was used for NMR relaxivity and DLS measurements. For chemical analysis, a portion of the diethylene glycol colloid was coagulated by the addition of ethyl acetate followed by magnetic separation, multiple washing of the precipitates with methanol and ethyl acetate, and drying in vacuum. Another portion was used for the preparation of oleate-capped nanopowders for TEM studies, XRD, and magnetic measurements. Precipitated magnetite oleate and maghemite oleate products were washed with methanol and dried in vacuum.

### 2.4. Analysis

The iron(II) to iron(III) ratio in the samples was determined by redox titration. Powdery samples (50–100 mg) were decomposed by dissolving in 10 mL of a 5% aqueous solution containing sulfuric and phosphoric acids (1:1) upon heating. The obtained clear solution was

analyzed by titration with 0.05 N $KMnO_4$. The amount of Fe(II) determined from this titration was compared to the total iron content determined by TGA analysis in an oxygen atmosphere (as $Fe_2O_3$).

## 3. Results and Discussion

It is known that the structure, surface composition, and metal ion site distribution in spinel-structured ferrite nanoparticles may vary depending on the synthesis method, and any deviation can significantly affect their magnetic properties. It was reasonable to hypothesize that such changes can also affect the NMR relaxivity properties of the nanoparticles. Because the aim of this work was to study the influence of the particle size and iron oxidation state on magnetic and NMR relaxivity properties, we deliberately attempted to prepare a series of samples whose crystal structure and surface chemistry were identical while the particle size and iron oxidation state were varied one at a time. To achieve this goal, we used synthesis methods based on the same chemistry for all of the products obtained. The parameters in the synthesis that were varied one at a time were the solution concentration and the reaction time and/or temperature. In all of the syntheses, the reaction stoichiometry was maintained with extreme care to ensure that the surface chemistry of the nanoparticles was identical in all batches.

Our synthesis strategy was based on the high-temperature hydrolysis of iron(II) and iron(III) chelated alkoxide complexes in solutions of the parent alcohol, diethylene glycol ($H_2$deg).

$$[\mathrm{Fe(Hdeg)_2}] + 2[\mathrm{Fe(Hdeg)(deg)}] + 4\mathrm{H_2O} \rightarrow \mathrm{Fe_3O_4} + 6\mathrm{H_2deg}$$

Formulas in this equation stand for nonisolated intermediate products, which form in diethylene glycol solutions of iron chlorides in the presence of base. (Evidence of their composition will be reported elsewhere.)

Magnetite nanoparticles were obtained as colloids stabilized by electrical double layers of the solvated ions and containing no capping ligands or surfactants, except for $H_2$deg. This surfactant-free colloidal system demonstrates remarkable stability; however, our earlier attempts to obtain magnetite particles with different sizes by changing the reaction conditions resulted in similarly sized or agglomerated products.[15] In the present work, we report the synthesis of $Fe_3O_4$ nanoparticles between 3.2 and 7.5 nm. We believe that this result was achieved by changing the Fe/$H_2O$ ratio from 1:6.67 in our earlier experiments to 1:1.56 in the current work. As a consequence, colloids with the lower water content in the current experiments are stable whereas colloids in our earlier experiments were coagulating by the end of the synthesis. All reactions and workup procedures were performed under an ultrapure nitrogen atmosphere in a glovebox (monitored oxygen content of 1–1.5 ppm) or with a Schlenk line. Regularly sized particles (4.8 nm) were obtained by injecting a concentrated diethylene glycol solution of the precursors into a pure solvent preheated to 245 °C. The temperature, which dropped to 190 °C after the injection, was maintained unchanged for 1 h. It was then increased to 210–220 °C and maintained at that level for another hour.

Smaller particles were obtained under milder conditions: the solvent was preheated to 220 °C. After the precursor solution's injection, the temperature dropped to 180 °C, and it was kept at this level for 1 h. Larger particles were obtained by a sequential growth method that consisted of several steps. The first step was identical to the synthesis of regular 4.8 nm nanoparticles. In the second step, a double portion of the precursor solution was added to the presynthesized colloid after it was cooled to ~100 °C. The reaction mixture was then held at

the temperature of 160 and 210 °C. This cycle was repeated twice under identical conditions.

Dynamic light scattering tests obtained for as-synthesized diethylene glycol colloids are presented in Table 1, along with results of the powder X-ray diffractometry and TEM. As can be seen, a minor fraction of the scattered light is attributed to objects larger than the reference nanoparticles. Taking into account that larger particles scatter light more strongly than small ones, the number of the larger particles in our colloids can be regarded as negligible. As we have also found, these aggregates usually break apart after the colloid is diluted with the parent solvent and left for 1 to 2 days.

Oleate-capped nanoparticles isolated as solids were used for XRD and magnetization experiments. Samples for TEM were prepared by the slow evaporation of toluene dispersions of oleate-coated particles deposited on a carbon grid. The representative XRDs are shown in Figure 1, and the TEM images are shown in Figure 2. More images, histograms and diffractograms can be found in the Supporting Information file (Figures S1– S6).

Iron(III) oxide colloids were obtained by the oxygenation of the parent magnetite colloid. This reaction was found to be slow at room temperature and was carried out by vigorous stirring of the starting colloid under a dry oxygen atmosphere at room temperature for 5–7 days. In the course of this reaction, the color of the colloid changed from brown-black to deep brown-orange. These colloids were examined by DLS and then by powder X-ray diffractometry and TEM after isolation of the oleate solids in a powdery state (Table 1).

Powder X-ray crystallography did not confirm the transition of magnetite to maghemite on the basis of the 0.3° difference in the 511 peak position[17] because this peak was too broad (Figures 1 and S5). To determine the degree of oxidation, we performed a chemical analysis on both the 4.8 nm particles of magnetite and on the product of its oxidation. Nanoparticulate solids were isolated from diethylene glycol colloids by precipitation with ethyl acetate, washing with methanol, and drying in vacuum. Because all of our powdery products contained a certain amount of the adsorbed diethylene glycol, the TGA method was used first to determine the exact content. The iron(II) content was determined by permanganate redox titration of the samples dissolved in a 5% aqueous 1:1 mixture of sulfuric and phosphoric acids. Prior to analysis, we determined that under the same conditions diethylene glycol undergoes oxidation much more slowly than does $Fe^{II}$ so that our titrations would be reliable. The average results obtained for several magnetite samples showed the ratio of $Fe^{II}/Fe^{III}$ to be 1:3.17; the oxidized samples showed this ratio to be 1: 50. Because $Fe^{II}$ oxidation in these samples was essentially complete, the analyzed products can be regarded as $Fe_2O_3$. Powder X-ray diffractometry provided the evidence that this oxide is spinel-structured, which identifies it as $\gamma$-$Fe_2O_3$ (maghemite).

The reduced content of iron(II) in magnetite samples can be attributed to partial oxidation during their isolation from the original colloids, associated with using large volumes of the washing solvents and with separation procedures. The samples of ligand-free magnetite are generally more oxygen-sensitive than those that are oleate-capped.

Samples for magnetic measurements were prepared as 5 wt % dispersions of the oleate-coated particles in a paraffin wax. This method of preparation helped to improve the accuracy in the sample load to protect the magnetite samples from oxidation and to minimize the interparticle magnetic interactions. The zero-field-cooled (zfc) and field-cooled (fc) magnetization curves were obtained for regularly sized (4.8 nm) oxidized and nonoxidized nanoparticles at a constant field of 50 Oe and in the temperature range of 4–300 K (Figure 3a,b). Both samples exhibited a blocking temperatures of 15 to 16 K. A magnetization study performed as a function of the magnetic field shows hysteretic behavior

at 5 K with a coercivity of 175 Oe for magnetite (Figure 4a,b) and 150 Oe for $\gamma$-iron(III) oxide. Remanent magnetization values are 19 and 13 emu/g, and the saturation magnetization values at 5 K and 50 kOe are 75 and 59 emu/g for $Fe_3O_4$ and $Fe_2O_3$, respectively. It is worth noting that the magnetization reaches 95% of its maximum value for magnetite and 97% of its maximum value for $\gamma$-iron(III) oxide in fields as low as 10 kOe. These values are approximately three-fourths of the saturation magnetization of bulk magnetite and maghemite (100 and 80 emu/g, respectively).[1] Somewhat greater values of the saturation magnetization and blocking temperature that we reported earlier[16] are likely to be attributed to the interparticle magnetic interaction in the samples prepared with no dilution.

As expected, the room-temperature curves show no coercivity or remanence, and the maximum magnetization values in a 50 kOe field reach 58 and 46 emu/g for 4.8 nm magnetite and $\gamma$-iron(III) oxide, respectively. The magnetization curves for 3.2 and 7.5 nm particles can be found in the Supporting Information (Figures S7–S10).

The effect of the particle size and iron oxidation state on the magnetic properties can be evaluated from the magnetization values obtained at room temperature and a field of 15 kOe, as presented in Table 2. As follows from these data, the larger particles of magnetite exhibit greater magnetization than smaller particles, and the magnetization value for $\gamma$-iron(III) oxide particles of the same size (4.8 nm) constitutes ~80% of the corresponding magnetization value for magnetite. These observations are expected and are in agreement with well-known trends.

Relaxivity NMR experiments were performed in pure diethylene glycol (Table 2) and in $D_2O$ (Table 3). Because $T_1$ relaxation experiments performed in this study could be strongly affected by the surface chemistry of iron oxide nanoparticles, the as-produced magnetite colloids were simply diluted with pure diethylene glycol. The only group of samples that went through a postsynthesis modification were the ones treated with dry oxygen. These samples are composed of $\gamma$-iron(III) oxide nanoparticles.

For diethylene glycol-based systems, we report two sets of $r_1$ values obtained for the protons of OH and $CH_2$ groups (Table 2). As can be seen, the relaxation of both OH protons and protons of $CH_2$ groups is strongly dependent on the particle size. The OH groups are involved in direct interactions with the surface of iron oxide nanoparticles, which enables the inner-sphere (spin–lattice) proton relaxation mechanism. The $CH_2$ protons of diethylene glycol can be regarded as second-sphere protons, which explains why their relaxation also appears to be strongly influenced.

There is a linear relationship between the $r_1$ values and the particle size for magnetite and $\gamma$-iron(III) oxide samples (Figure 5), with the slope being greater for OH protons. As considered for magnetite, the observed pattern correlates with the values of saturation magnetization of the corresponding particles.

Even though the saturation magnetization of $\gamma$-iron(III) oxide is ~20% lower than the saturation magnetization of magnetite, there is no distinct effect of this difference on the $r_1$ relaxivity values for most of the samples (Table 2). This result is rather unexpected, and the reason for this phenomenon is presently unknown. Because this is the case for both OH and $CH_2$ protons, we cannot attribute this fact to a specific interaction of the proton-bearing groups with $Fe^{III}$ or $Fe^{II}$ atoms on the nanoparticle surface. In conclusion, using $\gamma$-iron(III) oxide as an MRI contrast agent would be beneficial for practical purposes because it is chemically more stable and consequently less toxic.

To the best of our knowledge, no reports are available on the relaxivity studies involving diethylene glycol. We were interested, however, in finding a suitable reference system. The commonly used gadolinium diethylenetriaminepentaacetate (GdDTPA, magnevist) was found to be insoluble in diethylene glycol, so we could not use it directly as a reference. The $T_1$ and $T_2$ NMR experiments were performed with this complex dissolved in deuterium oxide, and the obtained results are in agreement with published relaxivity values in this solvent.[18] The behavior of $\gamma$-iron(III) oxide was also tested in dilute acidified $D_2O$ solutions. Prior to these tests, we checked and found that the rate of sample aggregation was slow compared to the time needed for the NMR experiment. This allowed us to perform a set of $T_1$ and $T_2$ experiments with 3.2, 4.8, and 7.5 nm $\gamma$-$Fe_2O_3$ (Table 3). The magnetite samples were not tested in $D_2O$ because of the high probability of their spontaneous oxidation in this solvent, which could not be used in a glovebox.

As evident from Table 3, the $r_2$ values are more strongly affected by the particle size than the $r_1$ values; consequently, the $r_2/r_1$ ratios decrease with the particle size. Since it is known that the magnitude of the outer-sphere relaxivity, $r_2$, for larger particles is greater because of their higher magnetic moment, our result is in agreement with this trend. These findings also provide evidence that smaller particles can be utilized as positive-contrast-enhancing MRI agents.

## 4. Conclusions

Uncoated magnetite and $\gamma$-iron(III) oxide nanoparticles from 3.2 to 7.5 nm in size were synthesized as stable diethylene glycol colloids. The nanocrystalline solids isolated from these colloids had a narrow size distribution based on TEM and X-ray powder diffractometry and high saturation magnetization values. The notable finding concerning their magnetic properties was that $\gamma$-iron(III) oxide particles have ~20% lower saturation magnetization than magnetite particles of the same size. The NMR relaxivity studies revealed similar longitudinal ($r_1$) relaxivity values for both types of particles and proved the smaller particles to have a smaller $r_2/r_1$ relaxivity ratio, which enhances their potential for use as MRI positive-contrast agents. On the basis of magnetic and relaxivity properties, the $\gamma$-iron(III) oxide particles would be even better candidates for this role because they are chemically more stable and consequently less toxic.

## Supplementary Material

Refer to Web version on PubMed Central for supplementary material.

## Acknowledgments

We thank Dr. Chin Lin and Prof. Marc Walters (New York University) for their help with the methodology of the relaxivity studies.

The research reported in this article was supported by the National Institutes of Health RCMI program under award number 8G12MD007595-04 and by the National Institute of General Medical Sciences of the National Institutes of Health under award number SC3GM088042. The content is solely the responsibility of the authors and does not necessarily represent the official views of the National Institutes of Health. This research was also supported by the Louisiana Cancer Research Consortium and the National Science Foundation (grants LA-SIGMA EPS-1003897 and PREM DMR-0934111).

## References

1. Cornell, RM.; Schwertmann, U. The Iron Oxides. Wiley-VCH; Weinheim, Germany: 2003.

2. Yuan Y, Rende D, Altan CL, Bucak S, Ozisik R, Borca-Tasciuc DA. Effect of Surface Modification on Magnetization of Iron Oxide Nanoparticle Colloids. Langmuir. 2012; 28:13051–13059. [PubMed: 22889238]

3. van Eldik, R.; Bertini, I., editors. Advances in Inorganic Chemistry. Vol. 57. Elsevier; San Diego, CA: 2005.

4. Campbell JL, Arora J, Cowell SF, Garg A, Eu P, Bhargava SK, Bansal V. Quasi-Cubic Magnetite/Silica Core-Shell Nanoparticles as Enhanced MRI Contrast Agents for Cancer Imaging. PLoS ONE. 2011; 6:e21857. [PubMed: 21747962]

5. Na HB, Palui G, Rosenberg JT, Ji X, Grant SC, Mattoussi H. Multidentate Catechol-Based Polyethylene Glycol Oligomers Provide Enhanced Stability and Biocompatibility to Iron Oxide Nanoparticles. ACS Nano. 2012; 6:389–399. [PubMed: 22176202]

6. Roch A, Muller RN. Theory of Proton Relaxation Induced by Superparamagnetic Particles. J Chem Phys. 1999; 110:5403–5411.

7. Lauffer RB. Paramagnetic Metal Complexes as Water Proton Relaxation Agents for NMR Imaging: Theory and Design. Chem Rev. 1987; 87:901–927.

8. Noginova N, Weaver T, King M, Bourlinos AB, Giannelis EP, Atsarkin VA. NMR and Spin Relaxation in Systems with Magnetic Nanoparticles. J Phys: Condens Matter. 2007; 19:1–10.

9. Penfield JG, Reilly RF Jr. What Nephrologists Need to Know about Gadolinium. Nat Clin Pract Nephrol. 2007; 3:654–668. [PubMed: 18033225]

10. Wan J, Jiang X, Li H, Chen K. Facile Synthesis of Zinc Ferrite Nanoparticles as Non-Lanthanide T1MRI Contrast Agents. J Mater Chem. 2012; 22:13500–13505.

11. Senpan A, Caruthers SD, Rhee I, Mauro NA, Pan D, Hu G, Scott MJ, Fuhrhop RW, Gaffney PJ, Wickline SA, Lanza GM. Conquering the Dark Side: Colloidal Iron Oxide Nanoparticles. ACS Nano. 2009; 3:3917–3926. [PubMed: 19908850]

12. Taboada E, Rodríguez E, Roig A, Oró J, Roch A, Muller RN. Relaxometric and Magnetic Characterization of Ultrasmall Iron Oxide Nanoparticles with High Magnetization. Evaluation as Potential $T_1$ Magnetic Resonance Imaging Contrast Agents for Molecular Imaging. Langmuir. 2007; 23:4583–4588. [PubMed: 17355158]

13. Babes L, Denizot B, Tanguy G, Le Jeune JJ, Jallet P. Synthesis of Iron Oxide Nanoparticles Used as MRI Contrast Agents: A Parametric Study. J Colloid Interface Sci. 1999; 212:474–482. [PubMed: 10092379]

14. Kim BH, Lee N, Kim H, An K, Park YI, Choi Y, Shin K, Lee Y, Kwon SG, Na HB, Park JG, Ahn TY, Kim YW, Moon WK, Choi SH, Hyeon T. Large-Scale Synthesis of Uniform and Extremely Small-Sized Iron Oxide Nanoparticles for High-Resolution $T_1$ Magnetic Resonance Imaging Contrast Agents. J Am Chem Soc. 2011; 133:12624–12631. [PubMed: 21744804]

15. Caruntu D, Caruntu G, Chen Y, O'Connor C, Goloverda G, Kolesnichenko VL. Synthesis of Variable-Sized Nanocrystals of $Fe_3O_4$ with High Surface Reactivity. Chem Mater. 2004; 16:5527–5534.

16. Goloverda G, Jackson B, Kidd C, Kolesnichenko V. Synthesis of the Ultrasmall Nanoparticles of Magnetic Iron Oxides and Study of Their Colloid and Surface Chemistry. J Magn Magn Mater. 2009; 321:1372–1376. [PubMed: 20161232]

17. Kim W, Suh CY, Cho SW, Roh KM, Kwon H, Song K, Shon IJ. A New Method for the Identification and Quantification of Magnetite-Maghemite Mixture Using Conventional X-ray Diffraction Technique. Talanta. 2012; 94:348–352. [PubMed: 22608459]

18. Siddiqui TS, Jani A, Williams F, Muller RN, Elst LV, Laurent S, Yao F, Wadghiri YZ, Walters MA. Lanthanide Complexes on Ag Nanoparticles: Designing Contrast Agents for Magnetic Resonance Imaging. J Colloid Interface Sci. 2009; 337:88–96. [PubMed: 19527906]

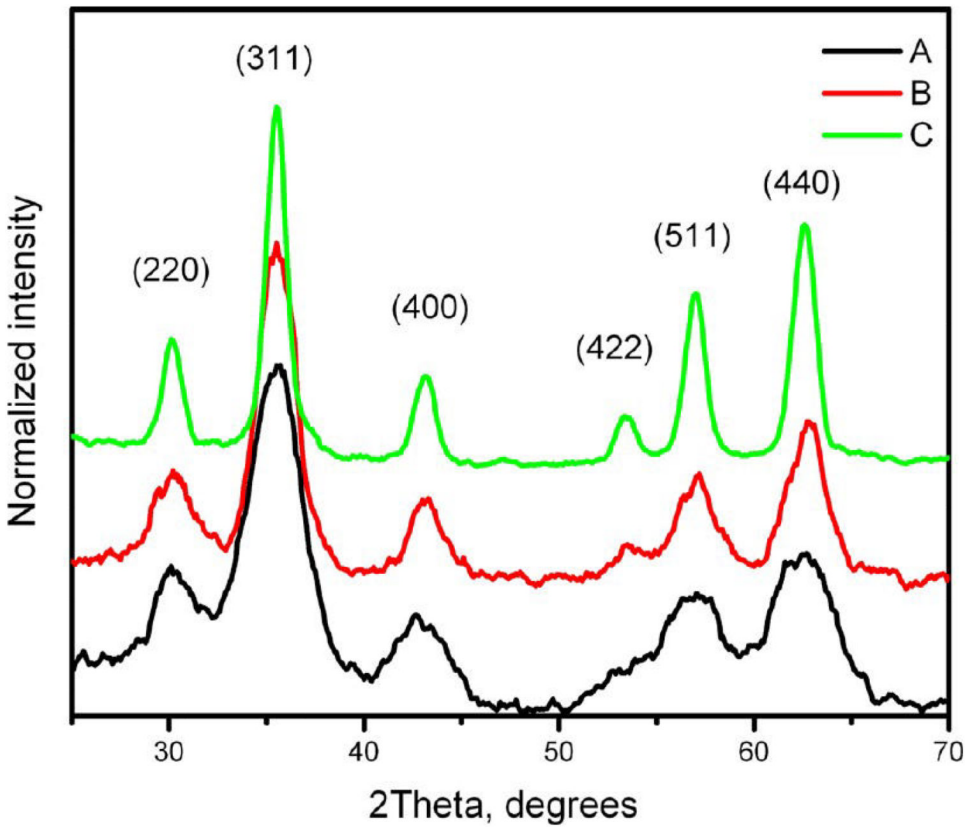


**Figure 1.**
Powder X-ray diffractograms for magnetite samples. The particle size was estimated using Scherrer's formula: (A) 2.9, (B) 3.9, and (C) 7.8 nm.

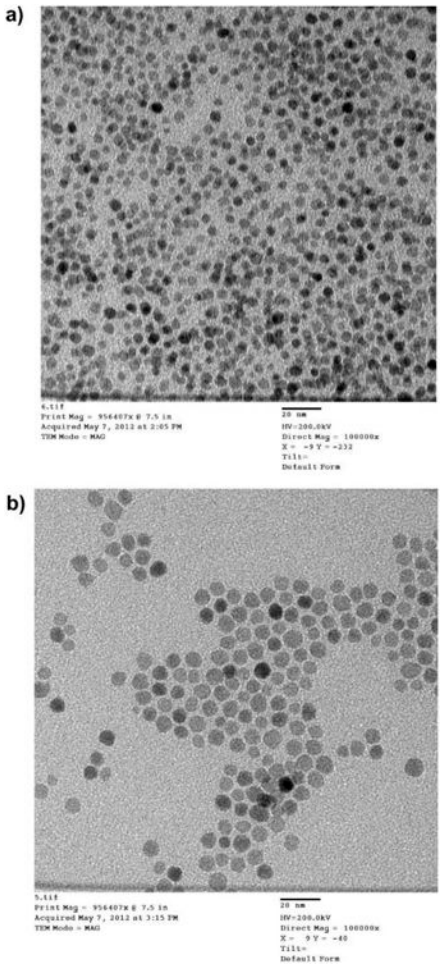


**Figure 2.**
(a) TEM image for a magnetite sample with a 4.8 nm particle size. Scale bar = 20 nm. (b) TEM image for a magnetite sample with a 7.5 nm particle size. Scale bar = 20 nm.

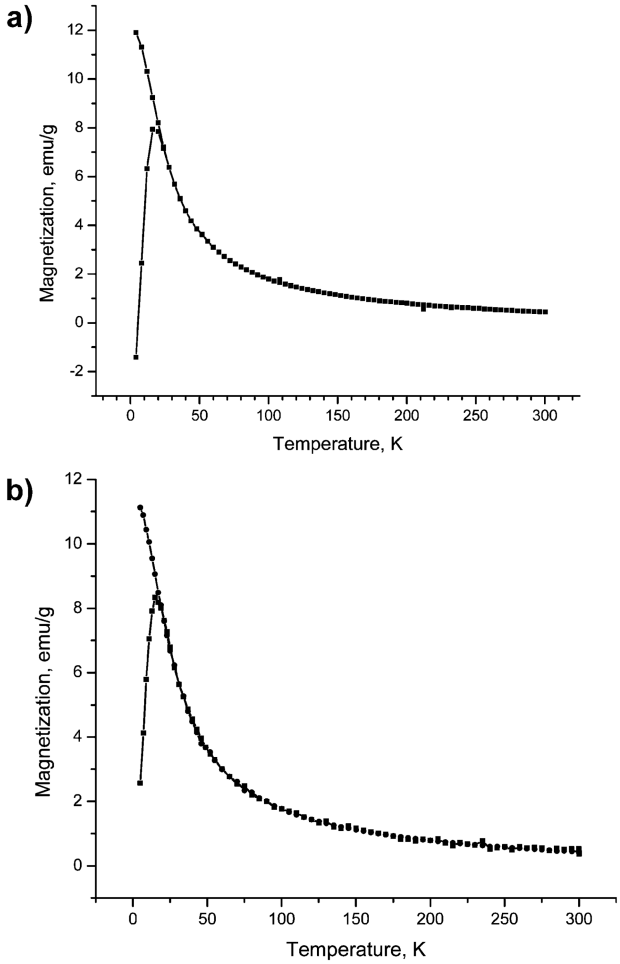


**Figure 3.**

(a) Zero-field-cooled (zfc) and field-cooled (fc) curves for 4.8 nm $Fe_3O_4$ particles in a 50 Oe field. (b) Zero-field-cooled (zfc) and field-cooled (fc) curves for 4.8 nm $\gamma$-$Fe_2O_3$ particles in a 50 Oe field.

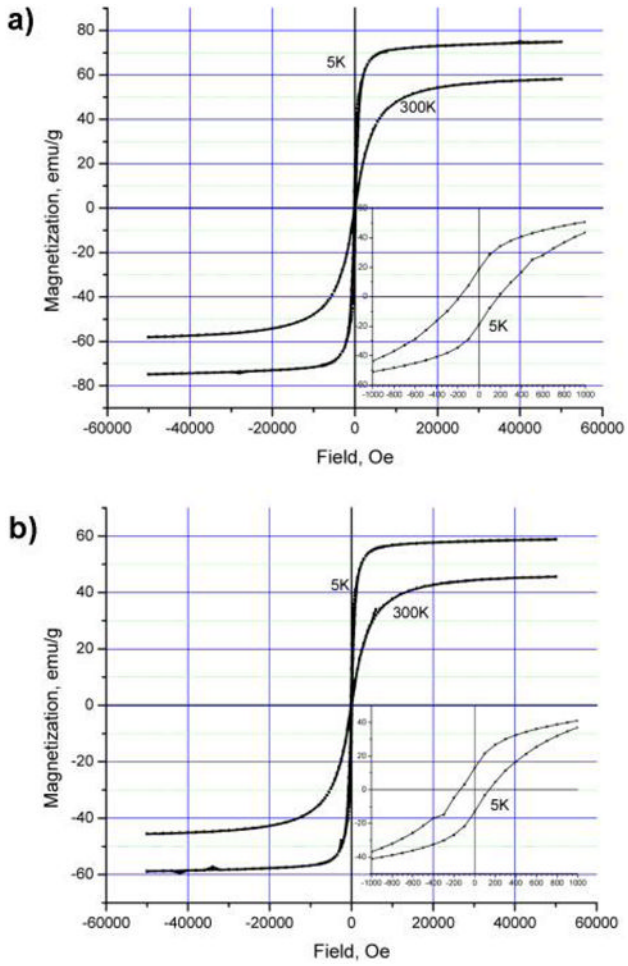


**Figure 4.**

(a) Magnetization curves for 4.8 nm $Fe_3O_4$ particles at different temperatures. (b) Magnetization curves for 4.8 nm $\gamma$-$Fe_2O_3$ particles at different temperatures.

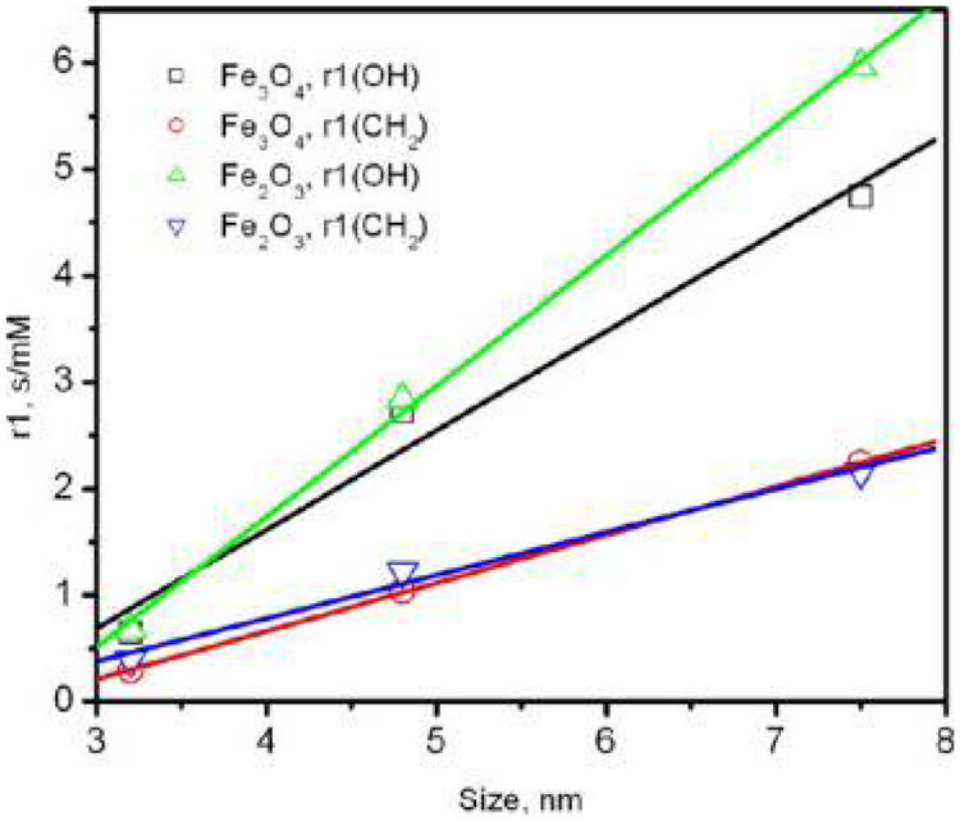


**Figure 5.**
Dependence of $r_1$ relaxivity values on the particle size.

## Table 1
### Summary of the Particle Size Determined by Different Physical Methods

| sample[a] | DLS (*d*, nm; %)[b] | XRD (*d*, nm) | TEM (*d*, nm; std %) |
|---|---|---|---|
| $Fe_3O_4$ 3.2 nm | 4.9; 67 | 2.9 | 3.19; 14 |
| $Fe_3O_4$ 4.8 nm | 7.2; 66 | 3.9 | 4.75; 16 |
| $Fe_3O_4$ 7.5 nm | 18.9; 100 | 7.8 | 7.5; 14 |
| $Fe_2O_3$ 3.2 nm | 5.1; 80 | 2.6 | |
| $Fe_2O_3$ 4.8 nm | 7.2; 80 | 5.4 | 4.80; 16 |

[a]The particle size in the sample code comes from TEM. The same codes are used in Table 2 and the text below.

[b]% intensity.

## Table 2

**Magnetization of the Particles Dispersed in Paraffin (at 300 K) and Relaxivity in Diethylene Glycol**

| | magnetization, emu/g[a] | | | |
|---|---|---|---|---|
| **sample** | **15 kOe** | **50kOe** | $r_1$**(OH)** | $r_1$**(CH$_2$)** |
| $Fe_3O_4$ 3.2 nm | 30 | 49 | 0.65 | 0.29 |
| $Fe_3O_4$ 4.8 nm | 52 | 58 | 2.72 | 1.04 |
| $Fe_3O_4$ 7.5 nm | 66 | 70 | 4.74 | 2.24 |
| $Fe_2O_3$ 3.2 nm | | | 0.68 | 0.39 |
| $Fe_2O_3$ 4.8 nm | 41 | 46 | 2.84 | 1.22 |
| $Fe_2O_3$ 7.5 nm | | | 5.97 | 2.16 |

[a]Per gram of pure iron oxide.

**Table 3**

**Relaxivity of $\gamma$-Iron(III) Oxide Nanoparticles and Magnevist in Deuterium Oxide**

| sample | $r_1$ | $r_2$ | $r_2/r_1$ |
|---|---|---|---|
| GdDTPA | 4.81 | 3.84 | 0.80 |
| $Fe_2O_3$ 3.2 nm | 3.00 | 23.75 | 7.92 |
| $Fe_2O_3$ 4.8 nm | 3.52 | 28.26 | 8.03 |
| $Fe_2O_3$ 7.5 nm | 10.8 | 204.2 | 18.91 |